Effect of P_2O_5 incorporated in slag on the hydration characteristics of cement-slag system

Zhang, Yu; Chen, Yu; Çopuroğlu, Oğuzhan

DOI
10.1016/j.conbuildmat.2023.131140

Publication date
2023

Document Version
Final published version

Published in
Construction and Building Materials

Construction and Building Materials 377 (2023) 131140

Contents lists available at ScienceDirect

Construction and Building Materials

journal homepage: www.elsevier.com/locate/conbuildmat

Effect of P_2O_5 incorporated in slag on the hydration characteristics of cement-slag system

Yu Zhang *, Yu Chen, Oğuzhan Çopuroğlu

Microlab, Section of Materials and Environment, Faculty of Civil Engineering and Geosciences, Delft University of Technology, Delft, The Netherlands

ARTICLE INFO

Keywords:
P_2O_5
Synthetic slag
Cement-slag system
Hydration products

ABSTRACT

This paper presents the influence of P_2O_5 incorporated in slag on the hydration characteristics of cement-slag system. It was found that the gradual addition of phosphorus oxide in slag did not change overall mineralogy of the hydration products. Except hydration retardation in the dormant stage, chemically bound water and portlandite contents, hydration degree of slag, and pore structure at all investigated ages were similar among cement-slag pastes with different P_2O_5 percentages. Furthermore, significantly higher amount of monosulfate was observed as the P_2O_5 content in slag increased. In addition, a higher Al/Si atomic ratio was measured in the C-S(A)-H gel phase formed in the cement matrix. However, similar Ca/Si atomic ratio of C-S(A)-H gel phase and Mg/Al atomic ratio of hydrotalcite-like phase were determined in all slag pastes, irrespective of the addition of P_2O_5. In contrast to magnesium ion which was retained within the original slag boundary, phosphorus ions could migrate into cement matrix. Therefore, P/Si atomic ratio of the C-S-H gel phase increased with the increasing phosphorus oxide content in slag, reaching up to ~0.08.

1. Introduction

To compensate the limited availability of raw material resources and the growing need for decreasing CO_2 emissions during cement and concrete productions, a practical way is to reduce the clinker proportion in cement. This strategy mainly consists of substituting a part of the clinker with supplementary cementitious materials (SCMs) at the cement and concrete production level [1–4]. These SCMs can be by-products from other industries, e.g., fly ash from coal power plants and blast furnace slag from steel-making industry, or natural materials, such as natural pozzolans.

Phosphorus slag is a by-product of yellow phosphor production via electrical furnace method. It is estimated that for each ton of yellow phosphorus, 7 tons of phosphorous slag are produced in general [5–8]. Several million tons of phosphorus slag was produced across the world annually [7,9], and it was commonly considered as a landfill waste, leading to serious environmental pollution. Phosphorous slag is mainly composed of CaO and SiO_2 (over 85 wt%), with small amounts of Al_2O_3 and P_2O_5 [7–11]. The glassy-phase content is higher than 90 wt% due to the high viscosity of molten slag, proving its potential chemical reactivity. The main crystalline compounds formed in phosphorus slag are $CaO{\cdot}SiO_2$, $3CaO{\cdot}2SiO_2$, and $3CaO{\cdot}2SiO_2{\cdot}CaF$, etc. [7,9].

It has been well demonstrated that phosphorus slag presents a similar reactivity to fly ash, and lower reactivity than blast furnace slag, probably owing to its lower Al_2O_3 content, as reported by [6,12]. The dissolution of phosphorous slag consumes portlandite and produces additional C-S-H gel phase, which can densify microstructure. However, phosphorous slag has not been widely used as SCMs in cement industry yet. The main concern is originated from the residual phosphorus in the form of P_2O_5 in phosphorous slag, resulting in delayed cement setting (retarding effect) [10,11].

However, the P_2O_5 content in phosphorous slag is low (typically <3 wt%), and its effect on slag reactivity has been overlooked. Moreover, very little is currently known about the influence of phosphorous on the formation of hydration products and its distribution after dissolution. Thus, this study aims to systematically investigate the impact of P_2O_5 incorporated in slag on the hydration characteristics of cement-slag system. Four synthetic slags produced in the laboratory with pure reagents were considered. One was made without any phosphorus-containing agents, the chemistry of which was representative of a typical commercial blast furnace slag in the market. Three phosphorous slags with increasing phosphorus oxide contents were also produced. To explore the effect of P_2O_5, the paper analyzed the kinetics of hydration, the evolution of hydration phase assemblage, and the development of

* Corresponding author.
E-mail addresses: Y.Zhang-28@tudelft.nl (Y. Zhang), Y.Chen-6@tudelft.nl (Y. Chen), O.Copuroglu@tudelft.nl (O. Çopuroğlu).

https://doi.org/10.1016/j.conbuildmat.2023.131140
Received 14 September 2022; Received in revised form 22 February 2023; Accepted 20 March 2023
Available online 23 March 2023

microstructure using a series of techniques. Additionally, the distribution of phosphorus in cement matrix and the influence of phosphorus oxide on slag reactivity were discussed. The authors believe that the results obtained in this paper propose new perspectives on utilizing phosphorus-rich slag in cement industry. Additionally, it provides insight into the interaction between cementitious materials and P_2O_5-containing admixtures, e.g., in [13–16].

2. Materials and methodology

2.1. Materials

CEM I 42,5N (manufactured by ENCI Maastricht B.V.), four synthetic slags, of which three (P3, P5, and P8) with and one (S) without phosphorus oxide, were employed in this study to produce the cement-slag system. Quartz was also introduced to act as a reference. The chemical compositions and selected physical properties of the raw materials are reported in Table 1. For these synthetic slags, CaO/SiO_2 ratio was kept at around 1, while the phosphorus oxide content increased from 3.11 (P3) to 8.32 wt% (P8). To eliminate the interference of Al_2O_3 and MgO, and avoid the introduction of other metal oxides, pure agent magnesium phosphate hydrate ($Mg_3(PO_4)_2{\cdot}H_2O$, provided by Sigma-Aldrich) was added as raw material to incorporate phosphorus oxide into slag. The Al_2O_3 and MgO contents were designed at ~14 and 8 wt%, respectively in the study. For the detailed process of slag production, the readers can refer to [17].

The particle size distribution of slags and quartz was measured by laser diffraction and is shown in Fig. 1. Fig. 2 shows the X-ray diffraction scan (XRD) of these slags. Apparently, they were entirely amorphous without any significant peak indicating crystallinity. No shift regarding the position of amorphous hump was observed, and it was centered at ~30° (2θ).

2.2. Mix design and experimental method

All raw materials were in mass percentage (wt.%) with respect to the total binder content (see Table 2). The slag (or quartz) to cement ratio was 7/3 and the water to binder ratio was 0.4. Mixtures were mixed at a high speed for 2 min, and then transported to 20 mL plastic bottles, which were sealed with thin parafilm to avoid any evaporation of water and ingress of CO_2. Sealed curing was performed for all specimens at room temperature until 3 months.

TAM Air isothermal calorimeter was employed to observe the heat evolution of paste sample at 20 °C for 7 days. The sample was prepared in the same manner mentioned above, and approximately 7 g of the binder was transported to a glass ampoule, sealed, and placed in the calorimeter.

Selective dissolution using a mixture of ethylenediaminetetraacetic acid (EDTA), Na_2CO_3 and triethanolamine was employed to calculate the reaction degree of slag in the hydrated paste with time, following the procedures suggested by [18]. Unreacted cement clinker, hydration products except hydrotalcite-like phase would be dissolved in the mixture solution, while unhydrated slag particle would not. At each sampling age, ~0.25 g of dry sample powder below 63 μm after

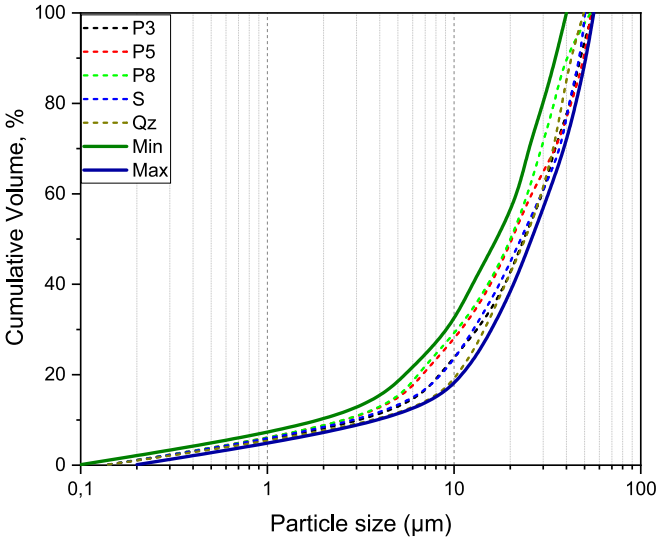

Fig. 1. Particle size distribution of slags and quartz.

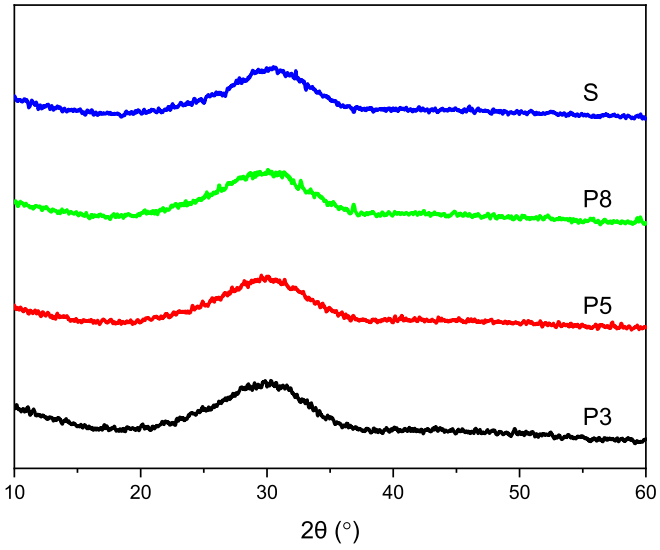

Fig. 2. XRD scan of slags used in the present research.

Table 1
Chemical compositions (wt.%) determined by XRF analysis and physical properties of cement and slags.

	Cement	P3	P5	P8	S
CaO	64	35.43	37.05	33.82	37.04
SiO_2	20	35.89	33.39	31.88	37.79
Al_2O_3	5	15.95	13.92	15.42	14.51
MgO	–	7.75	7.59	9.04	8.83
P_2O_5	–	***3.11***	***5.90***	***8.32***	–
FeO/Fe_2O_3	3	0.25	0.29	0.22	0.28
TiO_2	–	0.71	0.91	0.74	0.70
MnO/Mn_2O_3	–	0.16	0.17	0.16	0.17
Na_2O	0.58[a]	0.28	0.27	–	0.24
K_2O	–	0.26	0.27	0.22	0.25
SO_3	2.93	0.03	0.04	0.03	0.01
Residual	4.49	0.18	0.20	0.15	0.18
Physical properties					
d_{50} (μm)[b]	26.81	23.48	20.54	20.25	22.73
SSA (m^2/g)[c]	0.284	0.841	0.996	1.002	0.895

a. This value was determined as Na_2O_{eq} in cement, namely $Na_2O + 0.658 \times K_2O$.
b. The particle size distribution (PSD) of slags and quartz was measured by EyeTech, Ankersmid. The d_{50} of quartz is 24.21 μm.
c. The specific surface area (SSA) of cement and slags was measured by Blaine and nitrogen adsorption with the BET method respectively.

Table 2
Mixtures of specimen (g).

	Cement	Slag	Quartz	Water	w/b
Cement-slag	30	70	–	40	0.4
Cement-quartz	30	–	70	40	0.4

hydration stop was diluted in the mixture solution, shaken in a mechanical shaker for 1 h, and filtered through GF/C filter paper (The GF/C filter paper was dried at 105 °C oven for 1 h and weighed before testing). The residue on the filter paper was washed with deionized water several times and dried at 105 °C oven for 1 h before another weighing.

Before XRD and thermogravimetric analysis (TGA), hydration was stopped by solvent exchange with isopropanol. Slices cut from the specimen were crushed, ground, immersed in isopropanol for 15 min, filtered, and immersed for another 15 min. After filtration, sample powders were dried at 40 °C for ~8 min in a ventilated oven and then stored in a vacuum oven for further measurement. X-ray powder diffraction was performed on a Philips PW 1830/40 Powder diffractometer employing the Cu K-alpha radiation. The machine was operated with an acceleration voltage of 40 kV and an X-ray beam current of 40 mA. Analysis was performed with a step size of 0.03° for a 2θ range from 5° to 60°. Thermogravimetric analysis was carried out on Netzsch STA 449 F3 Jupiter under Argon atmosphere. About 40 mg of sample powder was heated from 40 to 900 °C with a heating rate of 10 °C/min in an Al_2O_3 crucible with an identical one as reference.

Fourier transform infrared spectroscopy was performed using Spectrum TM 100 Optical ATR-FTIR spectrometer over the wavelength range from 600 to 1600 cm^{-1} to identify the chemical bonding environment of Si structural unit. A single-beam configuration was used, and each sample was scanned 20 times with a fixed instrument resolution of 4 cm^{-1}.

Mercury intrusion porosimetry (MIP) measurement was also implemented to measure the pore size distribution of each mixture. The specimen was crushed into small slices, immersed in isopropanol solution to stop hydration, and stored under vacuum to constant weight subsequently. The maximum pressure applied by the instrument was 210 MPa, and each measurement process contained three steps: intrusion of mercury at a low pressure from 0 to 0.170 MPa; intrusion at a high pressure from 0.170 to 210 MPa and extrusion of mercury back to 0.170 MPa. The relationship between pore radius and pore pressure was elaborated in Washburn equation, of which the surface tension of mercury was 0.485 N/m at 25 °C and the contact angle between mercury and specimen was 140°.

Scanning electron microscopy (SEM) investigation was performed on selected samples, which had been dried at 40 °C, vacuum impregnated with epoxy resin, ground and polished by 9, 3, 1, and 0.25 μm diamond paste in turn. After each step, the samples were immersed briefly in an ultrasonic bath filled with 99.9 % ethanol for cleaning. The carbon coated sample was examined with FEI QUANTA FEG 650 ESEM at 10 kV accelerating voltage and 10 mm working distance to get backscattered secondary electron (BSE) image. Energy dispersive X-ray spectroscopy (EDS) point analysis was also used to determine the elemental composition of phase assemblage in the matrix and slag rim.

3. Result

3.1. Kinetics of hydration

3.1.1. Heat of hydration

Fig. 3 exhibits the heat evolution rate (a) and cumulative heat release (b) for all mixtures, normalized to per gram of cement. Note that a strong exothermic peak occurred upon contacting with water, which was ascribed to the initial dissolution of raw materials, especially C_3A ($3CaO•Al_2O_3$). The cement-quartz blend was dominated by one main hydration peak at approximately 12 h after mixing, related to the hydration of alite (C_3S, $3CaO•SiO_2$) in the cement clinker, and followed by a shoulder, implying the secondary aluminate reaction upon sulfate depletion [19,20].

During the dormant period, it was evident that the incorporation of slag containing phosphorus oxide prolonged the induction stage in comparison to that of slag S and Qz pastes. To be more specific, slag S and Qz mixtures entered accelerating stage at a similar timing, around 2 h after mixing, as the embedded graph shown in Fig. 3(a). However, the dormant stage was postponed by approximately 3, 4, and 4.5 h in slag *P*3, P5, and P8 systems, respectively, with the gradual addition of phosphorus oxide in slag. Commonly, there were two possible explanations regarding this retarding effect: (1) P_2O_5 in slag, even a minor amount, was able to react with Ca^{2+} ion and form $Ca_{10}(PO_4)_6(OH)_2$, resulting in the deficiency of Ca^{2+} ion in the pore solution and hindering the nucleation and growth of C-S-H gel phase and portlandite; (2) With slag dissolution, PO_4^{3-} ion tended to form phosphoric acid which would reduce the pH of pore solution, negatively affecting the hydration of cement clinker at an early age [6,9,21].

When stepping into the accelerating stage, the hydration rate of these mixtures was similar. The second aluminate reaction peak was observed clearly in slag S mixture soon after the main hydration peak, whereas it overlapped with the main hydration peak in slag P3, P5, and P8 pastes. Also, it was noted that this peak occurred earlier and was more intense in all slag blends when compared with that in cement-quartz blend (Fig. 3 (a)). Besides aluminate from C_3A, aluminum dissolved from slag also contributed to this enhanced secondary aluminate peak. Moreover, the possibility of a small number of reactions between small slag grain and

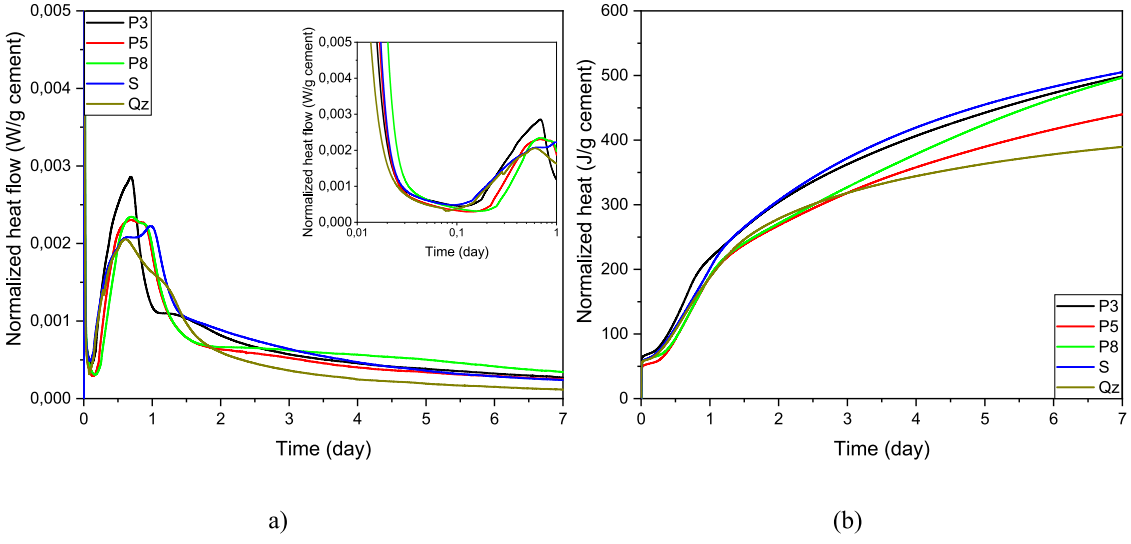

Fig. 3. Calorimetric curves of cement-slag and quartz systems. (a) Normalized heat flow; (b) Normalized heat release.

calcium hydroxide cannot be excluded, considering such a high slag replacement level [22–24].

The hump after the second aluminate reaction peak (after one day) could be distinguished among mixtures containing slag and quartz. This peak corresponded to the pozzolanic reaction between slag and portlandite. Moreover, continuous transformation of ettringite to calcium monosulfoaluminate (monosulfate for short) was also included in this hump until 7 days.

The curves of total heat release deviated from each other after 1 day, as Fig. 3(b) presents, indicating that slag started to participate in reaction from there on. Note that slag S, *P*3, and P8 mixtures evolved a similar heat, while ~50 J/(g cement) less heat was measured in slag P5 mixture at 7 days.

3.1.2. Chemically bound water and portlandite contents

Chemically bound water (BW) is assumed to be water chemically fixed in the hydrated phases and is often referred as non-evaporable water [25]. It is primarily associated with the amount of C-S-H gel phase formed in the matrix, which can be sourced from the hydration of cement clinker and pozzolanic reaction between portlandite and SCMs. According to the following formula [25], the bound water content of each mixture determined from TGA and corrected for the water bound in portlandite is present in Fig. 4(a):

$$BW = \left(\frac{W_{50} - W_{550} - W_{H_2OCH}}{W_{550}}\right) \times 100\%$$

with W_{50} = sample weight at 50 °C, W_{550} = sample weight at 550 °C, and $W_{H_2O\,CH}$ = mass loss from the dehydroxylation of portlandite by tangent method.

At all investigated ages, the bound water content of pastes containing slag was notably larger than that of cement-quartz paste. The gap increased with the prolongation of curing age because of the pozzolanic reaction. Besides, the gradual addition of P_2O_5 in slag increased the amount of bound water slightly, however, the difference was too small to distinguish.

Fig. 4(b) illustrates the portlandite content in the system with time. It was estimated based on the weight loss between 400 and 500 °C (dehydroxylation of portlandite) from TGA through the tangent method. This value can be regarded as an index indicating the hydration degree of slag (reactivity), as portlandite was mainly consumed in the pozzolanic reaction with slag. The portlandite content increased continuously in cement-quartz paste, although the increment was small after 7 days, meaning that most of cement clinker had been hydrated at this age. On the other hand, this value decreased from 7 days to 3 months in cement-slag mixtures, and the most and least portlandite contents were determined in slag P5 and P8 mixtures, respectively. Taking cement-quartz paste as a reference, it was calculated that about half (≈0.25/0.50) of portlandite liberated from cement hydration was consumed at 7 days and about one-third (≈0.15/0.50) was left at 90 days.

3.1.3. Selective dissolution

As mentioned earlier, the mixture solution allows the dissolution of unhydrated cement clinker, most hydration products except hydrotalcite-like phase. However, unhydrated slag particle cannot be dissolved through this procedure. The hydration degree of slag (α) in cement-slag system was calculated by comparing the residues after selective dissolution of unhydrated raw material (R_u) and hydrated sample powder (R_h) through the following equation:

$$\alpha = \frac{R_u - R_h}{R_u} \times 100\%$$

Moreover, a correction considering that Mg^{2+} dissolved from slag contributed to the formation of hydrotalcite-like phase was introduced following [26]:

$$\alpha_{correction} = \frac{R_u - R_h}{R_u \times (1 - hM)} \times 100\%$$

where h is 2.35, indicative of the mass of hydrotalcite-like phase formed from 1 g of MgO in slag and M (wt.%) was MgO content of slag.

This approach gives the results in Fig. 5. Slag P8 displayed the highest hydration degree at all investigated times, reaching ~0.2 at 90 days, close to the value measured in [27]. On the contrary, the hydration degree of slag P5 was the lowest, in agreement with the results of cumulative heat (Fig. 3(b)), as well as bound water and portlandite contents (Fig. 4). Similarly, the gap among slags was very small.

3.2. Hydration products

3.2.1. TG-DTG

TG-DTG curves of cement-slag and quartz systems after 7 days and 3 months of curing are shown in Fig. 6(a) and (b), respectively. Note that the main hydrates formed in slag-containing blends were similar. There were two distinct endothermic peaks on the DTG curve of all samples, corresponding to the water loss of C-S-H gel phase between 100 and 150 °C and the dehydroxylation of portlandite between 400 and 500 °C. Hydrotalcite-like phase could also be detected with a shoulder located at approximately 350 °C.

It was also noted that the shoulder at ~200 °C, implying the presence of monosulfate, was more visible in P_2O_5-containing slag pastes at all investigated ages when compared with that in slag S paste. The

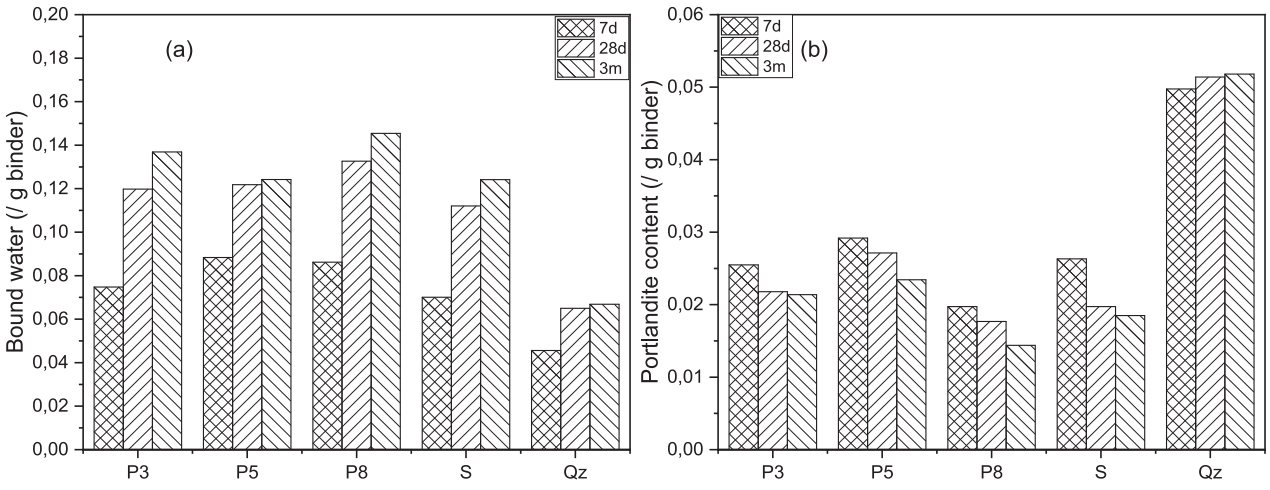

Fig. 4. (a) Bound water and (b) Portlandite contents of cement-slag and quartz systems.

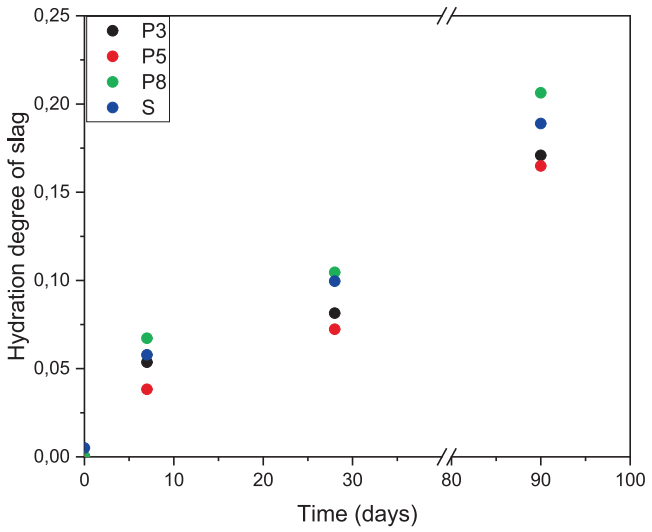

Fig. 5. Hydration degree of slags with respect to time based on selective dissolution method.

enrichment of monosulfate in P_2O_5-containing slag pastes was probably associated with the preferred release of aluminum from P_2O_5-containing slag (see Section 4.2). It was well recognized that in addition to aluminum incorporated into C-S(A)-H gel phase and hydrotalcite-like phase, aluminum dissolved from slag particles can also participate in the formation of monosulfate [28,29].

3.2.2. XRD

X-ray diffractograms in Fig. 7 reveal the presence of portlandite, unhydrated C_3S and C_2S in cement-slag mixtures at specific ages. As shown in the graph, the peak intensity of portlandite decreased from 7 days to 3 months, and the most negligible portlandite content was identified in slag P8 paste at 90 days, consistent with the results measured by TGA (Fig. 6(b)). No trace of ettringite was detected, and it suggested that the transformation from ettringite to monosulfate almost ended after 7 days of curing (Fig. 7(c)).

3.2.3. FTIR

Fig. 8 illustrates the FTIR spectra of cement-slag mixture at 90 days. Depending on the connectivity of silicon site in the $[SiO_4]^{4-}$ tetrahedral, silicate tetrahedral can be divided into five characteristic units further with representative IR absorption bands separately, i.e., Q^4 (~1200 cm^{-1}), Q^3 (~1100 cm^{-1}), Q^2 (~950 cm^{-1}), Q^1 (~900 cm^{-1}), and Q^0 (~850 cm^{-1}), respectively [30–33]. Apparently, Q^2 was the main unit of C-S-H gel phase of the investigated cement-slag pastes at 90 days, irrespective of the addition of P_2O_5 in slag or not. Moreover, no shift with respect to the position of Q^2 silicate group was observed, indicative of the similar polymerization degree of silicate chain in all investigated samples. The Q^0 unit was related to the silicate group that remained in

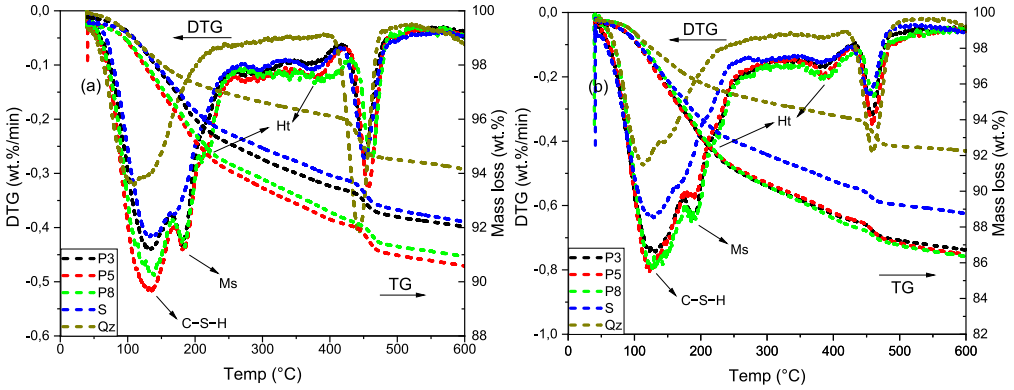

Fig. 6. TG-DTG curves of cement-slag and quartz systems after curing of (a) 7 days and (b) 3 months. Ms: calcium monosulfoaluminate; Ht: hydrotalcite-like phase.

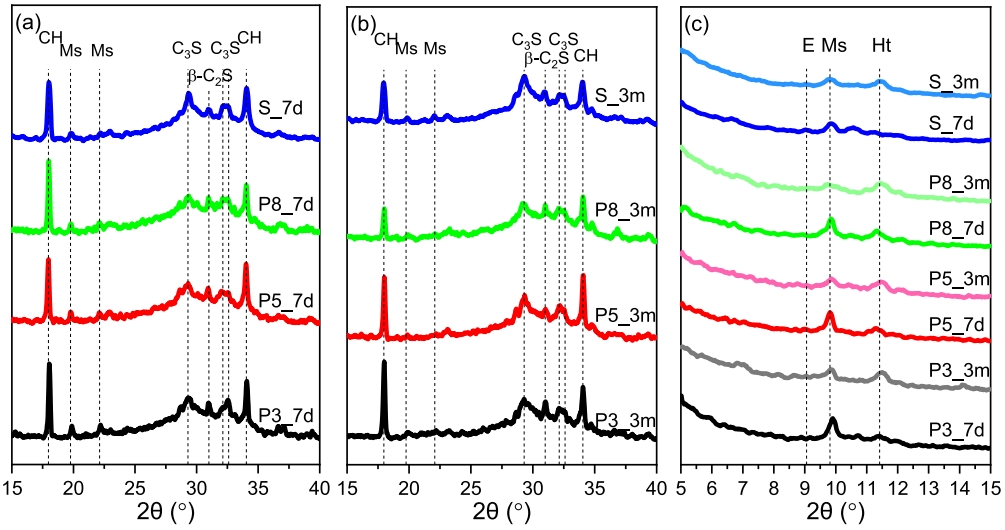

Fig. 7. XRD analysis of cement-slag systems after curing of (a) 7 days and (b) 3 months; (c) XRD patterns from 5 to 15° (2θ). E: ettringite; Ms: calcium monosulfoaluminate; Ht: hydrotalcite-like phase; CH: portlandite.

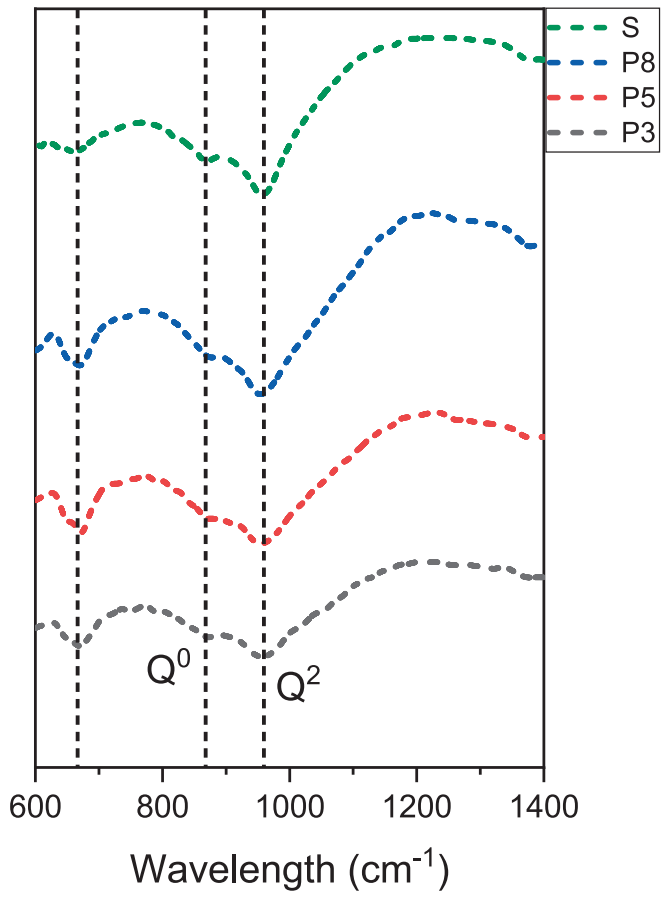

Fig. 8. FTIR spectra of cement-slag mixtures at 90 days.

unreacted slag particles.

Meanwhile, it was found that the band at around 650 cm^{-1}, ascribed to the asymmetric stretching vibration band of the $[AlO_4]^{5-}$ unit [34,35], was more intense in P_2O_5-containing slag pastes. Similarly, it was linked with the preferred release of aluminum from P_2O_5-containing slag, and thus more Al can be absorbed into C-S(A)-H gel phase (see Section 4.2).

3.3. Microstructure

3.3.1. Pore structure of the paste samples

Compared with cement-quartz mixture, hydrates formed from reaction between portlandite and slag helped refine the pore structure of slag pastes, which is illustrated clearly in Fig. 9. The critical pore radius decreased remarkably with curing time from 7 days to 3 months in all studied samples. At 7 days, cement-slag mixtures presented a bimodal pore structure; however, they eventually evolved into a unimodal pore structure at 90 days. Additionally, the critical pore radius of these cement-slag mixtures was almost identical after 3 months of curing, regardless of the addition or not of P_2O_5 in slag.

3.3.2. SEM-BSE

Fig. 10 exhibits the typical BSE micrographs of cement-slag mixtures after 3 months of curing. A close mixture of unhydrated slag grains, minor cement clinkers, hydrated phases and pores were observed to form the microstructure. Monosulfate (circled) existed as fine and compact clusters intermixed with C-S-H gel phase [36]. As confirmed in Section 3.2, more monosulfate was observed in P_2O_5-containing slag pastes, and it was distributed everywhere in the matrix. Also, the

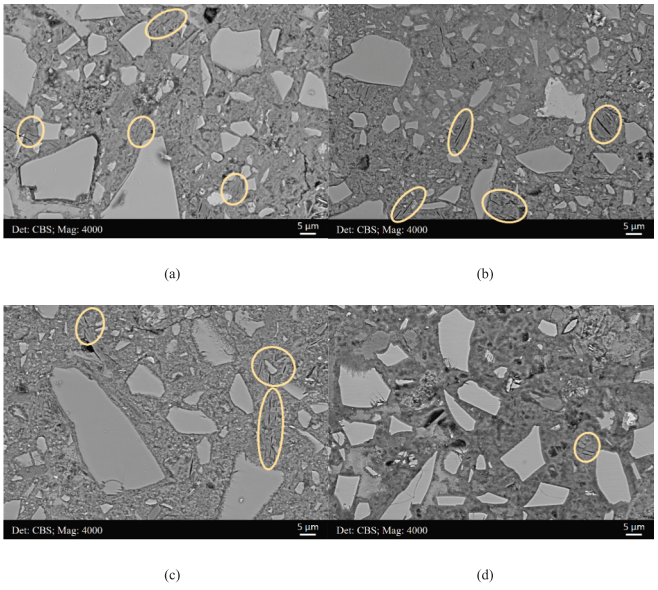

Fig. 10. Electron micrographs of typical cement-slag microstructure of (a) P3; (b) P5; (c) P8; and (d) S pastes after 3 months of curing.

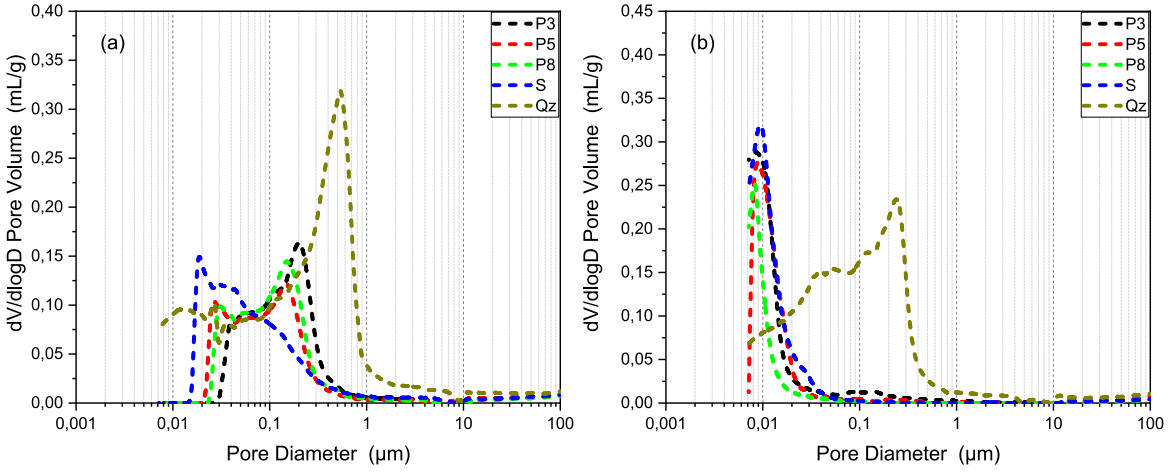

Fig. 9. Differential pore size distribution of samples measured after (a) 7 days and (b) 3 months of curing.

massive existence of unreacted slag particles indicated the slow hydration of slag.

3.3.3. Chemical composition of cement matrix

Hydration products in cement matrix and rims of unhydrated slag particles were characterized by SEM-EDS microanalysis with internal standards (standardless microanalysis). It was worth mentioning that the accelerating voltage used for analysis was 10 kV under high vacuum conditions.

The scatter plot of Al/Ca vs Si/Ca in molar ratio is presented in Fig. 11. The addition of phosphorus oxide in slag seemed to have no influence on the determined Ca/Si atomic ratio, which fluctuated at approximately 1.1, close to values reported in [28,37,38]. On the other hand, the Al/Si atomic ratio increased with phosphorus oxide incorporation. It agreed well with the FTIR results (Fig. 8) that an enhanced band at ~650 cm^{-1} was noted in phosphorus slag pastes. This can be ascribed to the asymmetric stretching vibration of $[AlO_4]^{5-}$ unit incorporated in C-S(A)-H gel phase. However, note that the trend was not very clear, and only some points in slag S paste tended to show a decreased Al/Si ratio. Thus, more point analysis was recommended in the future to verify this conclusion.

3.3.4. Chemical composition of slag rim

Hydrotalcite-like phase is the main precipitation from the hydration of slag, and its Mg/Al atomic ratio can be obtained from the slope of the regression line when plotting Mg/Si against Al/Si [28,39–41]. Fig. 12 presents the scatter plot of Mg/Si vs Al/Si in molar ratio. Note that the Mg/Al ratio of hydrotalcite-like phase formed in slag rim was nearly the same among slags, leveling off at ~1.60, commonly reported at high slag replacement levels [24,28,42].

4. Discussion

4.1. The distribution of phosphorus in cement matrix

As mentioned earlier, the P_2O_5 content in phosphorus slag was very low compared to the four main metal oxides (CaO-SiO_2-Al_2O_3-MgO), commonly <3 wt% [5–8]. At this level, P_2O_5 was always regarded as a minor or trace component, and few studies focused on its effect in depth.

To address this issue, we intentionally increased the amount of P_2O_5 in slag up to 8.32 wt% (P8), close to MgO. Fig. 13(a) and (b) give the EDS mappings of main elements (Ca, Si, and Mg + P) from the typical areas of slag P5 and P8 pastes, respectively. Ca appeared to be distributed over the whole region. Si deficiency was observed in some areas,

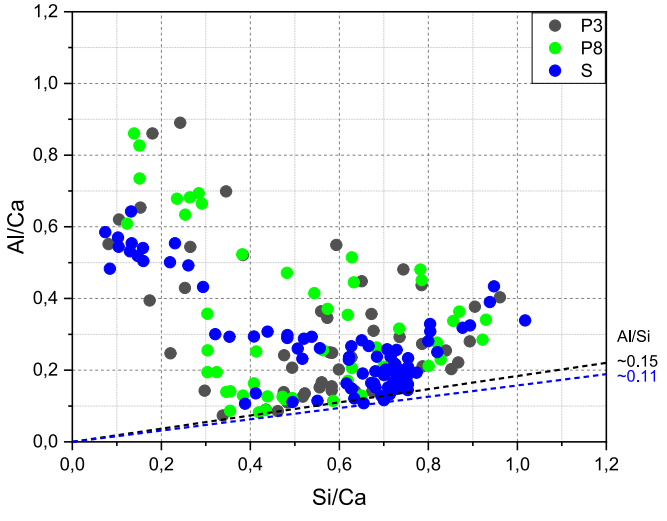

Fig. 11. Atomic ratio of Al/Ca against Si/Ca of cement-slag systems after 3 months of curing.

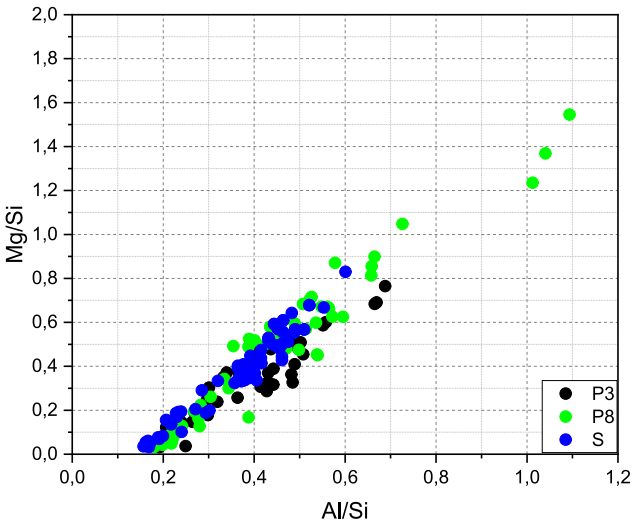

Fig. 12. Atomic ratio of Mg/Si against Al/Si of cement-slag systems after 3 months of curing.

characterized by the occupation of monosulfate. Compared with magnesium (yellow coloration) which was exclusively entrapped within the original slag grain boundaries, phosphorus (blue coloration) was able to migrate into cement matrix. It can be partially explained by the relatively high mobility of phosphate ion (In the strongly basic environment, e.g., the pore solution of blended cement paste, the phosphate ion (PO_4^{3-}) predominates [43].). Taking Mg^{2+} as a reference, the mobility of PO_4^{3-} was ~1.2 times higher [44].

Additionally, areas rich in phosphorus were also identified (circled in the graphs), where element phosphorus accumulated and formed clusters. The typical EDS spectra inside (Point 1) and outside (Point 2) these circles are displayed in Fig. 14(a) and (b), respectively. It was evident that these areas were rich in P, while the Si and Al concentrations decreased. The P/Si atomic ratio of Point 1 and 2 was 0.30 and 0.08, respectively. Probably it indicated the close mixture of C-S(A)-H gel phase and calcium phosphate hydrate ($Ca_3(PO_4)_2{\cdot}H_2O$) or hydroxyapatite ($Ca_5(PO_4)_3(OH)$) [13]. However, the existing characterization techniques cannot identify their precipitations due to the serious overlap with typical cement hydration products. One alternative method is to extract pore solution from the paste and measure concentrations of ions, including Ca^{2+}, Si^{4+}, Al^{3+}, Mg^{2+}, and PO_4^{3-}. According to the effective saturation index of various precipitations, the possible formations can thus be identified. These experimental results will be published in a follow up study.

Fig. 15 presents the scatter plot of P/Ca vs Si/Ca in molar ratio. For slag P3 paste, the P/Si ratio of cement matrix was quite low. On the other hand, the value was found to increase with the gradual addition of phosphorus oxide, which reached ~0.08 for slag P8 paste. Like silicate tetrahedral (SiO_4), each phosphorus atom can be surrounded by four oxygen atoms, forming phosphate tetrahedral (PO_4). Thus, P^{5+} is very suitable for the substitution of Si^{4+} and exhibits fourfold coordination to form PO_4 tetrahedral in the structure of C-S-H gel phase [45]. At this level (~0.08), phosphorus should have been incorporated into the gel, replacing silicon and forming C-S(A, P)-H. The works in [46,47] also confirmed that in the doping of C-S-H gel phase by P improved the stability of cement-based materials. From this point of view, the release of P from phosphorus slag was beneficial from cement matrix.

4.2. The effect of phosphorus oxide on the reactivity of slag

For commercial phosphorous slag from the production of yellow phosphorous, it mainly consists of CaO and SiO_2 with insufficient amounts of Al_2O_3 and MgO, fluctuating at 1 ~ 2 wt%, far less than that

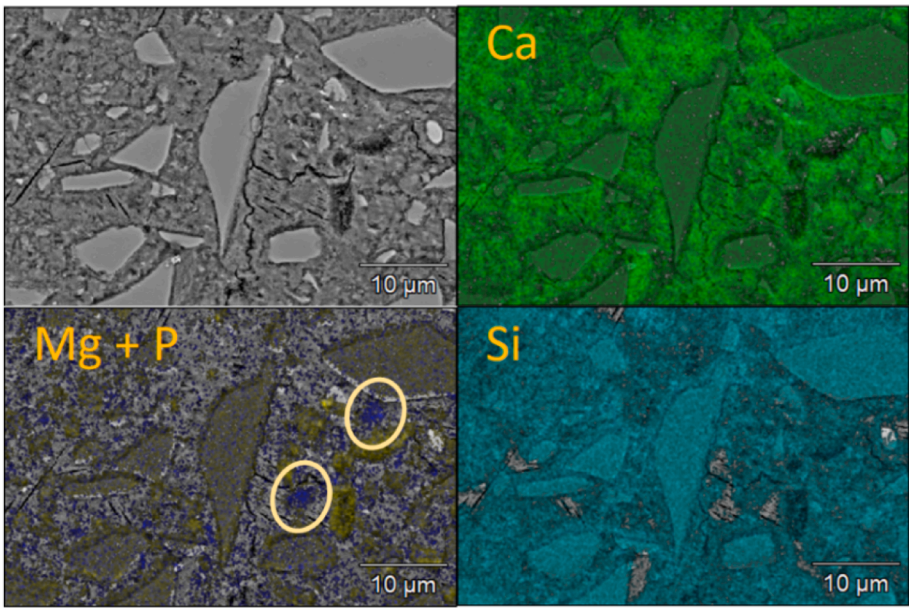

(a)

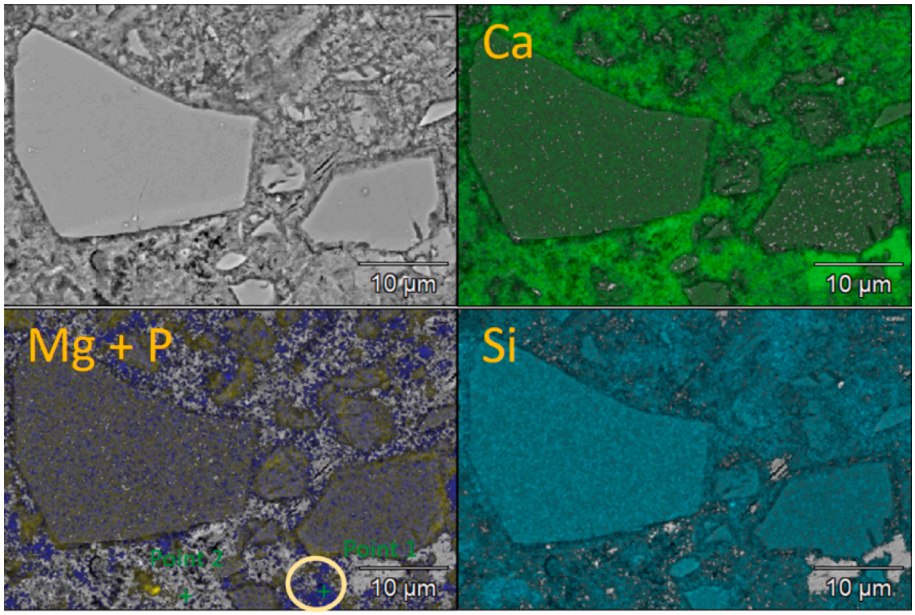

(b)

Fig. 13. Main EDS element mappings (a) P5; and (b) P8 slag pastes after 3 months of curing.

commonly encountered in blast furnace slag. Thus, it had been demonstrated that the low Al_2O_3 content reduced the reactivity of phosphorous slag [6,12]. According to the results found in [17], Al_2O_3 and MgO had a positive effect on slag reactivity, and low Al_2O_3 and/or MgO contents (<5 wt%) significantly decreased its reactivity. It explained the relatively low reactivity of slag P5 because of its lower Al_2O_3 and MgO contents.

To eliminate the interference of Al_2O_3 and MgO, the authors designed phosphorous slag with common Al_2O_3 and MgO contents in the study, i.e., about 14 and 8 wt%, respectively (see Table 1), and increased the phosphorus oxide content from 3.11 to 8.32 wt% gradually. For P_2O_5, it acts as a network former in the structure of glass [45]. Like silicate tetrahedral (SiO_4), each phosphorus atom is surrounded by four oxygen atoms, forming phosphate tetrahedral (PO_4). However, because of the excess charge of P^{5+}, phosphorus has three single bonds bound to other PO_4 units, and one double bond only connected with oxygen atom, named as non-bridge. Therefore, phosphate tetrahedral possesses a less cross-linked or polymerized structure than SiO_4 tetrahedral (Due to the absence of this double bond, SiO_4 tetrahedral exhibits a high degree of symmetry while phosphate tetrahedral is asymmetric [48].). Moreover, compared to Si-O-Si and Al-O-Al chains, P-O-P is much more easily hydrated, and phosphate glass typically has a poor water resistance [48–50]. Thus, except for the retarding effect during the dormant stage, the gradual addition of P_2O_5 in slag did not change the mineralogy of hydration phase assemblage. Similar bound water and portlandite contents, hydration degree of slag, pore structure, and chemical composition of hydration phase assemblage, at all investigated ages were achieved among cement-slag pastes with different P_2O_5 contents.

In the network structure of blast furnace slag, Al^{3+} is very suitable for the substitution of Si^{4+} and exhibits fourfold coordination to form AlO_4

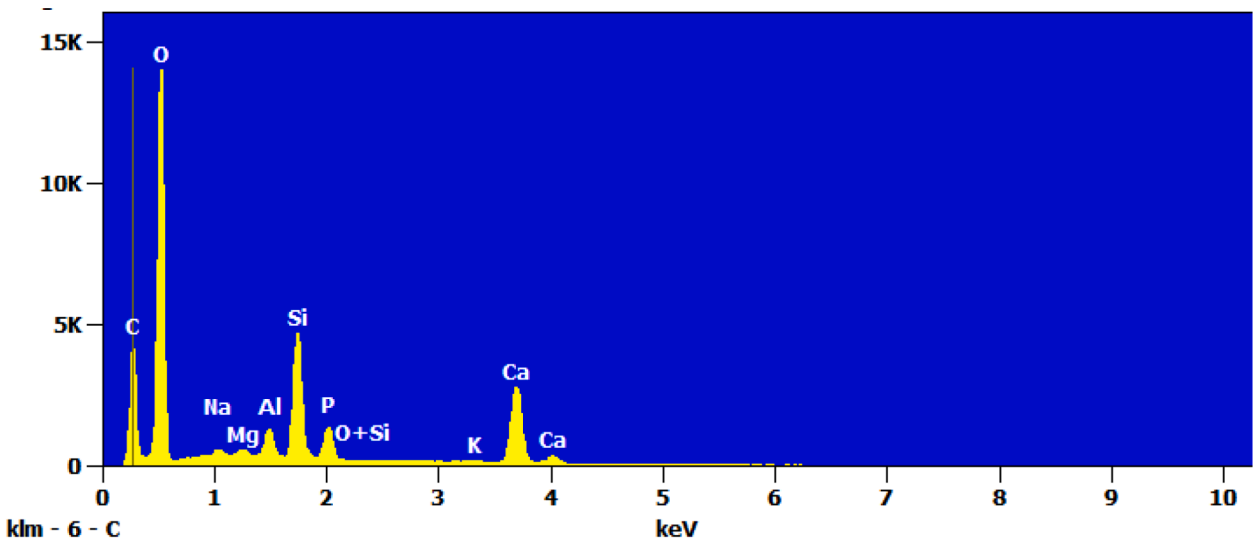

(a)

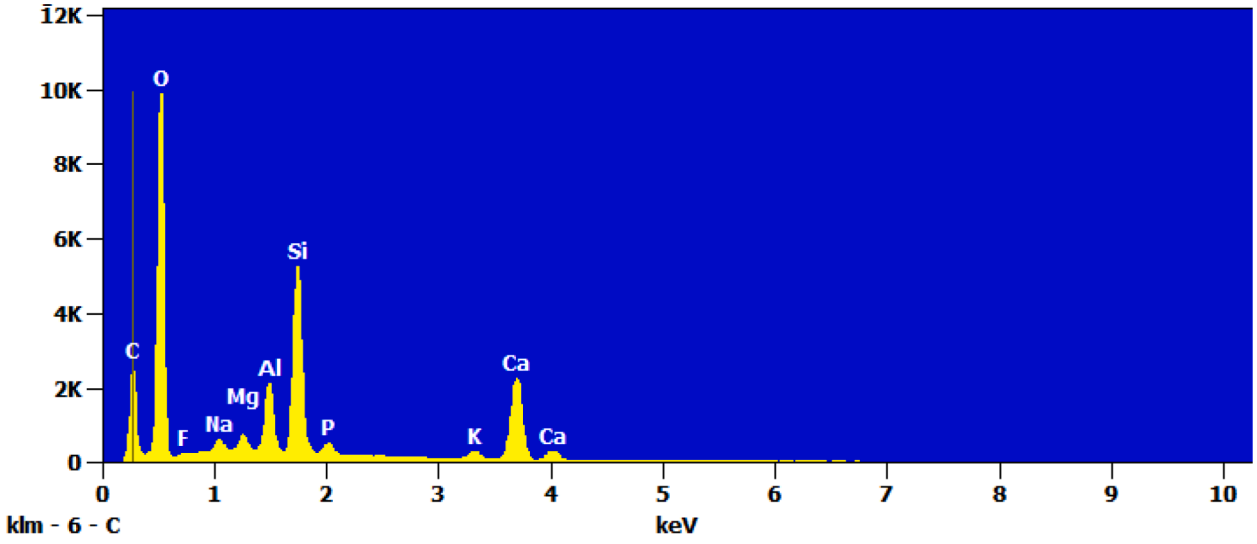

(b)

Fig. 14. Typical EDS spectra of points (a) inside (Point 1) and (b) outside (Point 2) circles in Fig. 13.

tetrahedral. The charge difference between AlO_4 and SiO_4 tetrahedras is balanced by cations in slag, Ca^{2+} and K^+ in principle [51,52]. However, it is noticed that fourfold coordinated Al (Al(IV)) was not favored in the aluminophosphate glass, while sixfold coordinated Al (Al(VI)) prevailed in the glass structure [53,54]. It is well recognized that Al(IV) is commonly considered as network former, while Al(V) and Al(VI) as network modifiers [55,56]. Under this circumstance, Al was more easily dissolved from phosphorus slag and moved into cement matrix, promoting the formation of monosulfate and involving in the substitution of Si in C-S(A, P)-H gel phase.

5. Conclusions

This paper presents the influence of P_2O_5 incorporated in slag on the hydration characteristics of cement-slag system. It was found that the gradual addition of phosphorus oxide in slag did not change overall mineralogy of the hydration products. The main conclusions drawn were as follows:

- Except hydration retardation in the dormant stage, chemically bound water and portlandite contents, hydration degree of slag, and pore structure at all investigated ages were similar among cement-slag pastes with different P_2O_5 dosages.
- Significantly higher amount of monosulfate was observed as the P_2O_5 content in slag increased. In addition, a higher Al/Si atomic ratio was measured in the C-S(A)-H gel phase formed in the cement matrix. It can be explained that Al(IV) was not favored in the aluminophosphate glass while Al(VI) prevailed, which was more easily hydrated. Thus, more Al can be dissolved from slag particles and move into cement matrix.
- Similar Ca/Si atomic ratio of C-S(A)-H gel phase and Mg/Al atomic ratio of hydrotalcite-like phase were determined in all slag pastes, irrespective of the addition of P_2O_5.
- In contrast to magnesium ion which was retained within the original slag boundary, phosphorus ions could migrate into cement matrix. The P/Si ratio of C-S-H gel phase was found to increase with the increasing phosphorus oxide content in slag, reaching ~0.08 for slag

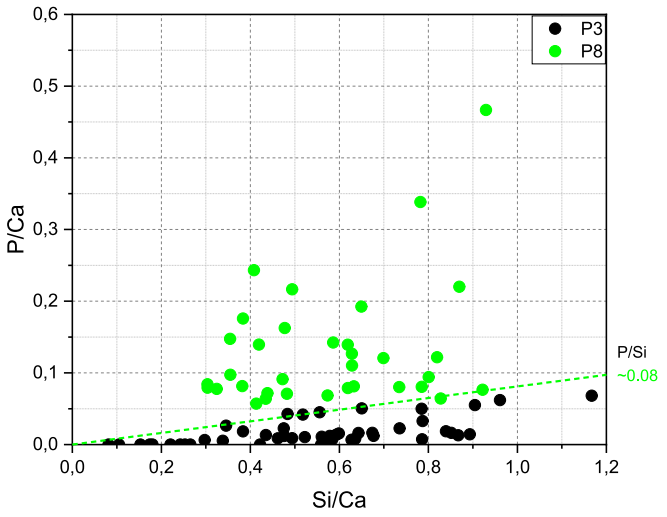

Fig. 15. Atomic ratio of P/Ca against Si/Ca of cement-slag P3 and P8 systems after 3 months of curing.

P8 paste. At this level, phosphorus should have been incorporated into the gel, replacing silicon and forming C-S(A, P)-H gel phase.

Based on results in the present paper, phosphorus-rich slag seems to be suitable for alkali-activated system, where fast setting is an issue. Also, the release of phosphorus and incorporation it into C-S-H gel phase improve the stability of cement-based materials, thus phosphorus-rich slag is beneficial for resisting deteriorations induced by environmental factors and improving the durability of cementitious materials.

CRediT authorship contribution statement

Yu Zhang: Investigation, Methodology, Writing – original draft, Writing – review & editing. **Yu Chen:** Writing – review & editing. **Oğuzhan Çopuroğlu:** Supervision, Funding acquisition, Writing – review & editing.

Declaration of Competing Interest

The authors declare that they have no known competing financial interests or personal relationships that could have appeared to influence the work reported in this paper.

Data availability

Data will be made available on request.

Acknowledgements

China Scholarship Council (the Grant Number 201808320456) and BAM Infraconsult B.V. are gratefully acknowledged for their financial support. Authors thank Arjan Thijssen (Microlab, TU Delft) for his technical support.

References

[1] M.C. Juenger, R. Siddique, Recent advances in understanding the role of supplementary cementitious materials in concrete, Cem. Concr. Res. 78 (2015) 71–80.
[2] E. Aprianti, A huge number of artificial waste material can be supplementary cementitious material (SCM) for concrete production–a review part II, J. Clean. Prod. 142 (2017) 4178–4194.
[3] K.H. Yang, Y.-B. Jung, M.-S. Cho, S.-H. Tae, Effect of supplementary cementitious materials on reduction of CO2 emissions from concrete, J. Clean. Prod. 103 (2015) 774–783.
[4] M.C. Juenger, R. Snellings, S.A. Bernal, Supplementary cementitious materials: New sources, characterization, and performance insights, Cem. Concr. Res. 122 (2019) 257–273.
[5] X. Chen, K. Fang, H. Yang, H. Peng, Hydration kinetics of phosphorus slag-cement paste, J. Wuhan Univ. Technol. 26 (1) (2011) 142–146.
[6] Z. Zhang, Q. Wang, J. Yang, Hydration mechanisms of composite binders containing phosphorus slag at different temperatures, Constr. Build. Mater. 147 (2017) 720–732.
[7] R. Yang, et al., Low carbon design of an Ultra-High Performance Concrete (UHPC) incorporating phosphorous slag, J. Clean. Prod. 240 (2019), 118157.
[8] Y. Peng, J. Zhang, J. Liu, J. Ke, F. Wang, Properties and microstructure of reactive powder concrete having a high content of phosphorous slag powder and silica fume, Constr. Build. Mater. 101 (2015) 482–487.
[9] A. Allahverdi, S. Pilehvar, M. Mahinroosta, Influence of curing conditions on the mechanical and physical properties of chemically-activated phosphorous slag cement, Powder Technol. 288 (2016) 132–139.
[10] H. Mehdizadeh, E.N. Kani, Rheology and apparent activation energy of alkali activated phosphorous slag, Constr. Build. Mater. 171 (2018) 197–204.
[11] D. Li, J. Shen, L. Mao, X. Wu, The influence of admixtures on the properties of phosphorous slag cement, Cem. Concr. Res. 30 (7) (2000) 1169–1173.
[12] P. Gao, X. Lu, C. Yang, X. Li, N. Shi, S. Jin, Microstructure and pore structure of concrete mixed with superfine phosphorous slag and superplasticizer, Constr. Build. Mater. 22 (5) (2008) 837–840.
[13] O. Çopuroğlu, A. Fraaij, J. Bijen, Effect of sodium monofluorophosphate treatment on microstructure and frost salt scaling durability of slag cement paste, Cem. Concr. Res. 36 (8) (2006) 1475–1482.
[14] K.L. Lin, D. Lin, H. Luo, Influence of phosphate of the waste sludge on the hydration characteristics of eco-cement, J. Hazard. Mater. 168 (2–3) (2009) 1105–1110.
[15] A. Papo, L. Piani, R. Ricceri, *Sodium tripolyphosphate and polyphosphate as dispersing agents for kaolin suspensions: rheological characterization*, Colloids Surfaces A: Physicochem. Eng. Aspects 201 (1–3) (2002) 219–230.
[16] P. Swift, H. Kinoshita, N.C. Collier, C.A. Utton, Phosphate modified calcium aluminate cement for radioactive waste encapsulation, Adv. Appl. Ceram. 112 (1) (2013) 1–8.
[17] Y. Zhang, et al., The effect of slag chemistry on the reactivity of synthetic and commercial slags, Constr. Build. Mater. 335 (2022), 127493.
[18] V. Kocaba, E. Gallucci, K.L. Scrivener, Methods for determination of degree of reaction of slag in blended cement pastes, Cem. Concr. Res. 42 (3) (2012) 511–525.
[19] A. Quennoz, K.L. Scrivener, Interactions between alite and C3A-gypsum hydrations in model cements, Cem. Concr. Res. 44 (2013) 46–54.
[20] F. Zunino, K. Scrivener, Factors influencing the sulfate balance in pure phase C3S/C3A systems, Cem. Concr. Res. 133 (2020) 106085.
[21] S. Liu, L. Wang, B. Yu, Effect of modified phosphogypsum on the hydration properties of the phosphogypsum-based supersulfated cement, Constr. Build. Mater. 214 (2019) 9–16.
[22] Gruyaert, E., et al., Study of the hydration of Portland cement blended with blast-furnace slag by calorimetry and thermogravimetry. 2010. 102(3): p. 941-951.
[23] Y. Zhang, Z. Wan, L.M. de Lima Junior, O. Çopuroğlu, Early age hydration of model slag cement: Interaction among C3S, gypsum and slag with different Al2O3 contents, Cem. Concr. Res. 161 (2022) 106954.
[24] Y. Zhang, E. Schlangen, O. Çopuroğlu, Effect of slags of different origins and the role of sulfur in slag on the hydration characteristics of cement-slag systems, Constr. Build. Mater. 316 (2022), 125266.
[25] R. Snellings, et al., Rapid, robust, and relevant (R3) reactivity test for supplementary cementitious materials, ACI Mater. J. 116 (4) (2019).
[26] K. Luke, F.P. Glasser, Selective dissolution of hydrated blast furnace slag cements, Cem. Concr. Res. 17 (2) (1987) 273–282.
[27] J.I. Escalante, L.Y. Gómez, K.K. Johal, G. Mendoza, H. Mancha, J. Méndez, Reactivity of blast-furnace slag in Portland cement blends hydrated under different conditions, Cem. Concr. Res. 31 (10) (2001) 1403–1409.
[28] R. Taylor, I. Richardson, R. Brydson, Composition and microstructure of 20-year-old ordinary Portland cement–ground granulated blast-furnace slag blends containing 0 to 100% slag, Cem. Concr. Res. 40 (7) (2010) 971–983.
[29] K. Luke, E. Lachowski, *Internal composition of 20-year-old fly ash and slag-blended ordinary Portland cement pastes*, J. Am. Ceram. Soc. 91 (12) (2008) 4084–4092.
[30] B.O. Mysen, et al., The influence of TiO2 on the structure and derivative properties of silicate melts, Am. Mineral. 65 (11–12) (1980) 1150–1165.
[31] Y. Sun, Z. Zhang, L. Liu, X. Wang, FTIR, Raman and NMR investigation of CaO–SiO2–P2O5 and CaO–SiO2–TiO2–P2O5 glasses, J. Non Cryst. Solids 420 (2015) 26–33.
[32] G.H. Kim, I. Sohn, Effect of Al2O3 on the viscosity and structure of calcium silicate-based melts containing Na2O and CaF2, J. Non Cryst. Solids 358 (12–13) (2012) 1530–1537.
[33] S.M. Han, J.-G. Park, I.l. Sohn, Surface kinetics of nitrogen dissolution and its correlation to the slag structure in the CaO-SiO2, CaO-Al2O3, and CaO-SiO2-Al2O3 slag system, J. Non Cryst. Solids 357 (15) (2011) 2868–2875.
[34] B.T. Poe, P.F. McMillan, C.A. Angell, R.K. Sato, Al and Si coordination in SiO2-Al2O3 glasses and liquids: A study by NMR and IR spectroscopy and MD simulations, Chem. Geol. 96 (3-4) (1992) 333–349.
[35] S. Zhang, X.i. Zhang, W. Liu, X. Lv, C. Bai, L. Wang, Relationship between structure and viscosity of CaO–SiO2–Al2O3–MgO–TiO2 slag, J. Non Cryst. Solids 402 (2014) 214–222.
[36] K.L. Scrivener, Backscattered electron imaging of cementitious microstructures: understanding and quantification, Cem. Concr. Compos. 26 (8) (2004) 935–945.

[37] I. Richardson, Tobermorite/jennite-and tobermorite/calcium hydroxide-based models for the structure of CSH: applicability to hardened pastes of tricalcium silicate, β-dicalcium silicate, Portland cement, and blends of Portland cement with blast-furnace slag, metakaolin, or silica fume, Cem. Concr. Res. 34 (9) (2004) 1733–1777.
[38] J.I. Escalante-Garcia, J. Sharp, The chemical composition and microstructure of hydration products in blended cements, Cem. Concr. Compos. 26 (8) (2004) 967–976.
[39] Y. Zhang, O. Çopuroğlu, The role of hydrotalcite-like phase and monosulfate in slag cement paste during atmospheric and accelerated carbonation, Cem. Concr. Compos. 132 (2022) 104642.
[40] Y. Zhang, M. Liang, Y. Gan, O. Çopuroğlu, Effect of MgO content on the quantitative role of hydrotalcite-like phase in a cement-slag system during carbonation, Cem. Concr. Compos. 134 (2022) 104765.
[41] Y. Zhang, O. Çopuroğlu, The effect of slag chemistry on CO2 binding capacity of C3S-slag (-gypsum) system, Constr. Build. Mater. 354 (2022) 129208.
[42] M. Whittaker, M. Zajac, M. Ben Haha, F. Bullerjahn, L. Black, The role of the alumina content of slag, plus the presence of additional sulfate on the hydration and microstructure of Portland cement-slag blends, Cem. Concr. Res. 66 (2014) 91–101.
[43] B. Da Silva Cerozi, K. Fitzsimmons, The effect of pH on phosphorus availability and speciation in an aquaponics nutrient solution, Bioresour. Technol. 219 (2016) 778–781.
[44] Speight, J.G., Lange's handbook of chemistry. 2017: McGraw-Hill Education.
[45] R.K. Brow, The structure of simple phosphate glasses, J. Non Cryst. Solids 263 (2000) 1–28.
[46] V.O. Ozçelik, C.E. White, Nanoscale charge-balancing mechanism in alkali-substituted calcium–silicate–hydrate gels, J. Phys. Chem. Lett. 7 (24) (2016) 5266–5272.
[47] R. Dupuis, J.S. Dolado, J. Surga, A. Ayuela, Doping as a way to protect silicate chains in calcium silicate hydrates, ACS Sustain. Chem. Eng. 6 (11) (2018) 15015–15021.
[48] U. Hoppe, A structural model for phosphate glasses, J. Non Cryst. Solids 195 (1–2) (1996) 138–147.
[49] X. Yu, D.E. Day, G.J. Long, R.K. Brow, Properties and structure of sodium-iron phosphate glasses, J. Non Cryst. Solids 215 (1) (1997) 21–31.
[50] S. Reis, M. Karabulut, D. Day, Chemical durability and structure of zinc–iron phosphate glasses, J. Non Cryst. Solids 292 (1–3) (2001) 150–157.
[51] B.O. Mysen, D. Virgo, F.A. Seifert, The structure of silicate melts: implications for chemical and physical properties of natural magma, Rev. Geophys. 20 (3) (1982) 353–383.
[52] B.O. Mysen, Relationships between silicate melt structure and petrologic processes, Earth Sci. Rev. 27 (4) (1990) 281–365.
[53] H. Liu, Y. Lu, Y. Qu, H. Lu, Y. Yue, Effect of the content of Al2O3 on structure and properties of calcium-phosphate glasses: two experimental case studies, J. Non Cryst. Solids 450 (2016) 95–102.
[54] A.E. Marino, S.R. Arrasmith, L.L. Gregg, S.D. Jacobs, G. Chen, Y. Duc, Durable phosphate glasses with lower transition temperatures, J. Non Cryst. Solids 289 (1-3) (2001) 37–41.
[55] C.I. Merzbacher, B.L. Sherriff, J.S. Hartman, W.B. White, A high-resolution 29Si and 27Al NMR study of alkaline earth aluminosilicate glasses, J. Non Cryst. Solids 124 (2-3) (1990) 194–206.
[56] D.R. Neuville, L. Cormier, D. Massiot, Al coordination and speciation in calcium aluminosilicate glasses: Effects of composition determined by 27Al MQ-MAS NMR and Raman spectroscopy, Chem. Geol. 229 (1-3) (2006) 173–185.